UNCERTAINTY-BASED EXTENSIBLE CODEBOOK FOR DISCRETE FEDERATED LEARNING IN HETEROGENEOUS DATA SILOS

Anonymous authors
Paper under double-blind review

ABSTRACT

Federated learning (FL), aimed at leveraging vast distributed datasets, confronts a crucial challenge: the heterogeneity of data across different silos. While previous studies have explored discrete representations to enhance model generalization across minor distributional shifts, these approaches often struggle to adapt to new data silos with significantly divergent distributions. In response, we have identified that models derived from FL exhibit markedly increased uncertainty when applied to data silos with unfamiliar distributions. Consequently, we propose an innovative yet straightforward iterative framework, termed *Uncertainty-Based Extensible-Codebook Federated Learning (UEFL)*. This framework dynamically maps latent features to trainable discrete vectors, assesses the uncertainty, and specifically extends the discretization dictionary or codebook for silos exhibiting high uncertainty. Our approach aims to simultaneously enhance accuracy and reduce uncertainty by explicitly addressing the diversity of data distributions, all while maintaining minimal computational overhead in environments characterized by heterogeneous data silos. Through experiments conducted on various datasets, our method has demonstrated its superiority, achieving significant improvements in accuracy (by 3%–22.1%) and uncertainty reduction (by 38.83%–96.24%), thereby outperforming contemporary state-of-the-art methods.

1 INTRODUCTION

Federated Learning (FL), well known for its capacity to harness data from diverse devices and locations—termed data silos—while ensuring privacy, has become increasingly crucial in the digital era, particularly with the explosion of data from mobile sources. Despite its pivotal role in distributed computing, FL confronts a formidable challenge: the heterogeneity of data across different silos. Such diversity often results in a significant performance gap when integrating updates from local models into the global model. In Fig. 1, we compare the mean accuracy of local FL models with that of the global model after integration when addressing data silos with different distributions. While local models may perform impressively within their own data domains, the aggregated global model often struggles to achieve similar performance levels after synthesizing updates from these varied data sources. This issue is especially pronounced in FL due to its reliance on varied data sources.

Recent studies (Ghosh et al., 2020; Agarwal et al., 2021; Liu et al., 2021; Kairouz et al., 2021a; Zhang et al., 2022; Yuan et al., 2022) have made significant advancements in addressing data heterogeneity within Federated Learning (FL), with one notable approach being the use of discrete representations to enhance model robustness against minor data shifts. Nonetheless, this strategy struggles to generalize models to data silos exhibiting significant distributional differences. Furthermore, these methods face difficulties in adapting to unseen data distributions, as they typically require the entire model to be re-trained. Such constraints limit their flexibility in adapting to the dynamically changing data landscapes, posing challenges for their applicability in real-world scenarios.

Moreover, we identify another critical issue impacting the model's performance across diverse data silos: increased uncertainty, as shown in Fig. 1. The global model's accuracy not only deteriorates,

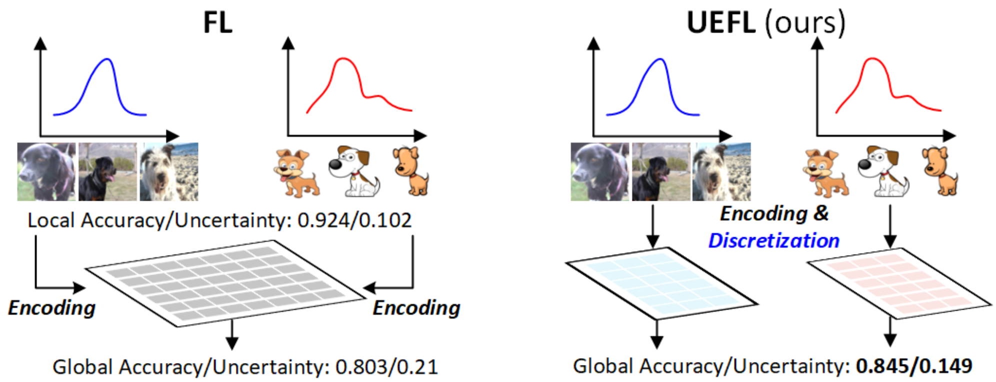

Figure 1: In the case of heterogeneous data silos, the global model of regular Federated Learning (FL) performs poorly compared to local models before integration. By discretizing different domains into distinct latent spaces, our UEFL improves both accuracy and uncertainty. The reported values in the figure represent the average accuracy and uncertainty across the various data silos.

but its uncertainty also trends upwards, signaling increased prediction instability. To address these challenges, we introduce Uncertainty-Based Extensible-codebook Federated Learning (UEFL), a novel methodology that explicitly distinguishes between data distributions to improve both accuracy and uncertainty.

Specifically, our design features an advanced codebook comprising a predetermined number of latent vectors (*i.e*. codewords), and employs a discretizer to assign encoded image features to their closest codewords. These codewords, acting as latent representations, are passed to subsequent layers for processing. The codewords are dynamically trained to align with the latent features generated by the image encoder. To mitigate performance degradation when integrating local models from data silos with varying distributions, we initialize a small, shared codebook for all clients. Additional specific codewords are then introduced for individual client use, ensuring explicit differentiation between them. Since the initial codebook is small and requires only a few extensions, the final size remains compact, minimizing the associated computational overhead. Given the privacy constraints in federated learning (FL), which restrict direct data access, we incorporate an uncertainty evaluator using Monte Carlo Dropout. This evaluator identifies data from diverse distributions, marked by high uncertainty. During training, our UEFL method systematically distinguishes between these varied distributions and dynamically adds new codewords to the codebook until all distributions are sufficiently represented. In the initial training cycle, shared codewords are randomly initialized. However, in subsequent cycles, the fully trained image encoder is leveraged to initialize new codewords using K-means, aligning them more closely with the data distribution and facilitating faster adaptation to various distributions. As a result, our UEFL model can accommodate data from previously unseen distributions with fewer communication rounds, making it applicable for enhancing other FL algorithms. Furthermore, since uncertainty constantly decreases as training progresses, the iterative process is guaranteed to conclude after a few iterations.

To summarize, our contributions are as follows:

- We identify a significant increase in model uncertainty across silos with diverse data distributions within the federated learning (FL) context, highlighting the challenge of data heterogeneity.
- To address this heterogeneity, we introduce an extensible codebook approach that distinguishes between data distributions by stepwise mapping them to distinct, trainable latent vectors (*i.e*. codewords). This methodology allows for efficient initialization of newly added codewords using a K-means algorithm, closely aligning with the training data feature distributions and enabling rapid convergence during codebook training.
- We propose a novel data-driven FL framework, named Uncertainty-Based Extensible-codebook Federated Learning (UEFL), which merges the extensible codebook with an uncertainty evaluator. This framework iteratively identifies data from diverse distributions by

assessing uncertainty without requiring direct data access. It then processes this data by initializing new codewords to complement the existing codebook, ensuring that each iteration focuses on training the expandable codebook, which rapidly converges, thus allowing UEFL to adapt seamlessly to new data distributions.

- Our empirical evaluation across various datasets demonstrates that our approach significantly reduces uncertainty by 38.83%-96.24% and enhances model accuracy by 3%-22.1%, evidencing the effectiveness of UEFL in managing data heterogeneity in FL.

2 Related Work

2.1 Federated Learning

Federated learning (Konečnỳ et al., 2016; Geyer et al., 2017; Chen et al., 2018; Hard et al., 2018; Yang et al., 2019; Ghosh et al., 2020) represents a cutting-edge distributed learning paradigm, specifically designed to exploit data and computational resources across edge devices. The Federated Averaging (FedAvg) algorithm (McMahan et al., 2017), introduced to address the challenges of unbalanced and non-IID data, optimizes the trade-off between computation and communication costs by reducing the necessary communication rounds for training deep networks. Federated Learning (FL) faces numerous statistical challenges, with data heterogeneity being one of the most critical. In real-world applications, data collected across different clients often varies significantly in terms of distribution, feature space, and sample sizes.

Several methodologies (Zhao et al., 2018; Li et al., 2018; 2019; Kalra et al., 2023) have been developed to address this pivotal issue. PMFL (Zhang et al., 2022) approaches the heterogeneity challenge by drawing inspiration from meta-learning and continual learning, opting to integrate losses from local models over the aggregation of gradients or parameters. DisTrans (Yuan et al., 2022) enhances FL performance through train and test-time distributional transformations, coupled with a novel double-input-channel model architecture. Meanwhile, FCCL (Huang et al., 2022) employs knowledge distillation during local updates to facilitate the sharing of inter and intra domain insights without compromising privacy, and utilizes unlabeled public data to foster a generalizable representation amidst domain shifts. Additionally, the discrete approach to addressing heterogeneity by Liu et al. (2021), provide further inspiration and valuable perspectives for our research endeavors.

2.2 Uncertainty

Recently, the study of uncertainty modeling has gained significant prominence across various research fields, notably within the machine learning community (Chen et al., 2014; Blundell et al., 2015; Kendall & Gal, 2017; Louizos & Welling, 2017; Lahlou et al., 2021; Nado et al., 2021; Gawlikowski et al., 2021). This surge in interest is driven by the critical need to understand and quantify the inherent ambiguity in complex datasets. Techniques such as Monte Carlo Dropout (Gal & Ghahramani, 2016), which introduces variability in model outputs through the use of dropout layers, and Deep Ensembles (Lakshminarayanan et al., 2017), which leverages multiple models with randomly initialized weights trained on identical datasets to evaluate uncertainty, exemplify the advancements in this area. Furthermore, the application of uncertainty modeling has extended beyond traditional domains, impacting fields such as healthcare (Dusenberry et al., 2020) and continual learning (Ahn et al., 2019).

3 Methodology

3.1 Overall Architecture

Fig. 2 illustrates the workflow of our UEFL. Consider multiple data distributions $\mathcal{D}_1, \mathcal{D}_2, ..., \mathcal{D}_M$, with data samples $x \in \mathbb{R}^{H \times W \times D}$, where H, W, and D denote the input image's height, width, and channel count, respectively, drawn from these M distributions. Upon distributing the global model to local clients, data samples undergo local encoding via a shared encoder θ_E into feature representations $z \in \mathbb{R}^{h \times w \times d}$, with h, w, and d representing the features' shape. Subsequently, these features are reshaped into vectors $z \in \mathbb{R}^{l \times d}$, where l is the number of tokens, and divided into

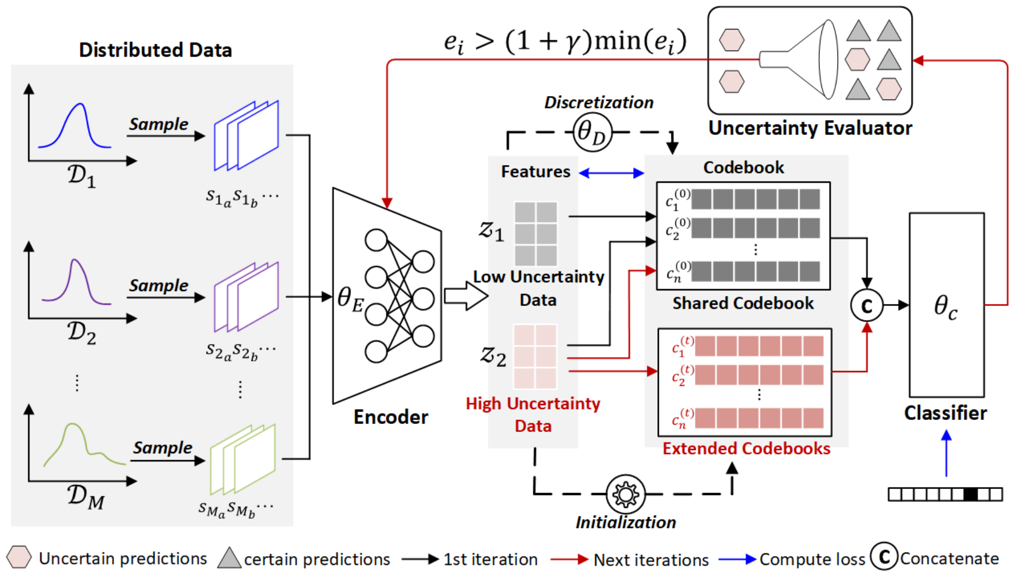

Figure 2: **UEFL flowchart.** In the first iteration, all latent are mapped to initialized shared codewords by the discretizer θ_D. In the next iterations, UEFL identifies data from heterogeneous distributions with the uncertainty evaluator, and complements new codewords with K-means initialization to enhance the codebook. Clients with high uncertainty can select not only newly added codewords but also shared codewords.

s segments $z_i \in \mathbb{R}^{l \times \frac{d}{s}}, \forall i$, with s indicating the segment count. Each segment is mapped to the closest codeword in the codebook via a discretizer θ_D, then reassembled into complete vectors for classification. The classifier θ_C then deduces the class for the input data, completing the forward processing sequence as follows,

$$z = f_{\theta_E}(x), \quad c = f_{\theta_D}(z), \quad p = f_{\theta_C}(c) \tag{1}$$

where x, z, c, and p denote input data, latent features, discrete coded vectors, and the model prediction, separately.

After loss calculation, models undergo local updates through backpropagation. In a manner akin to FedAvg (McMahan et al., 2017), these updated models are then relayed back to the server for a global update.

$$\theta_k \leftarrow \theta - \eta g_k, \ \forall k \tag{2}$$

$$\theta \leftarrow \sum_{k=1}^{K} \frac{n_k}{n} \theta_k, \tag{3}$$

where θ denots the global model parameters, θ_k is the kth local model parameters, g_k is the kth model gradients, n_k is the number of samples for data silo k, and n is the total number of samples for all K silos.

At the end of each iteration, assessing uncertainty through Monte Carlo Dropout is essential, given the privacy constraints of Federated Learning (FL), which limit direct access to client data. By evaluating uncertainty against a pre-established threshold, we identify data from heterogeneous distributions. When such data are detected, we augment the codebook with v new codewords initialized by K-means. These newly generated codewords are then exclusively accessible to the corresponding heterogeneous clients, updating the codebook size for the kth client from v_k to $v_k + v$., as described in Algorithm 1. This process leverages the fully adapted encoder from previous iterations, utilizing K-means to ensure the new codewords are closely aligned with the actual data distribution, thereby facilitating faster convergence during training. Additionally, since the extended codewords are specific to individual client data and are not included in the integration with other local models, our method ensures that latent features from different distributions remain explicitly differentiated. Consequently, the global model performs better after integration, effectively handling data heterogeneity.

Algorithm 1 Uncertainty-Based Extensible-Codebook Federated Learning (UEFL)

Input: data distributions $\mathcal{D}_1$, $\mathcal{D}_2$, ..., $\mathcal{D}_M$
Parameters: uncertainty threshold γ, learning rate η, codewords loss weight β
Sample K data silos from $\mathcal{D}_1$, $\mathcal{D}_2$, ..., $\mathcal{D}_M$ as clients
Randomly initialize model parameters θ and codebook with v codewords
Initially assign uncertainty for all clients to be zero: $e_k = 0, \forall k$
repeat
  for each round t = 1, 2, ... **do**
    Broadcast θ to all clients
    for all K clients **in parallel do**
      if $e_k > (1+\gamma)\min_{\forall j \in 1,2,...,K}(e_j)$ **then**
        K-means initialize another v codewords and add them to codebook
        Update accesible codewords size for clients with high uncertainty: $v_k \leftarrow v_k + v$
      end if
      Encode input into latent features: $z = f_{\theta_E}(x)$
      Discretize latent features to codewords c_i, where $i = argmin_{j \in 1,2,...,v_k} ||z - c_j||_2$
      Predict with coded vectors: $p = f_{\theta_C}(c_i)$
      Compute codewords loss: $\mathcal{L}_{code} = ||sg(c_i) - z||_2^2 + \beta||c_i - sg(z)||_2^2$
      Compute output loss: $\mathcal{L}_{task} = -\sum y \log p$
      Update local parameters with gradient descent: $\theta_k \leftarrow \theta_k - \eta \nabla_\theta(\mathcal{L}_{code} + \mathcal{L}_{task})$
    end for
    Clients return all local models θ_k to the server
    Update the server model $\theta \leftarrow \sum_{k=1}^{K} \frac{n_k}{n} \theta_k$
  end for
  Evaluate uncertainty for each client with integrated model: $e_k = \sum p \log p$
  Reduce the number of communication rounds
until $e_k \leq (1+\gamma)\min_{\forall j \in 1,2,...,K}(e_j), \forall k$

3.2 Extensible Codebook

To effectively manage heterogeneous data, we design an extensible codebook, beginning with a minimal set of codewords and progressively enlarging this set through a superior initialization strategy that benefits from our UEFL framework. This strategy facilitates stepwise mapping of diverse data distributions to distinct codewords. Starting with a larger codebook can introduce uncertainty in codeword selection due to the concurrent training of multiple codewords.

Similar to VQ-VAE (Van Den Oord et al., 2017), we employ latent vectors as codewords, initializing a compact shared codebook with n codewords $c \in \mathbb{R}^{n \times \frac{d}{s}}$, where n represents the size of the initial codebook. The codewords are initialized using a Gaussian distribution and shared across all data silos. After each iteration's uncertainty assessment, we determine which silos require additional codewords to improve prediction accuracy, and we extend the codebook accordingly for these silos by adding n more codewords.. The newly added codewords are initialized using K-means, leveraging the encoder's improved latent features from the prior iteration to better align with the underlying data distribution. To optimize codebook usage, data silos that demonstrated lower performance in the previous iteration are allowed to select codewords from both the newly added codewords and the original shared codebook. Typically, the codebook only requires 1-3 extensions until all clients reach low uncertainty levels. The server updates the codebook by computing the average of codewords across the clients that utilize those specific codewords.

For a given iteration, if the codebook size for the kth client is v_k, the feature vector z is associated with a codeword c_i by the discretizer, which computes the distance between z and all available codewords, selecting the nearest one as follows,

$$i = \underset{j \in 1,2,...,v_k}{\arg\min} ||z - c_j||_2 \tag{4}$$

K-means Initialization. After the first iteration, the adapted encoder produces image features that more accurately reflect the distribution of the training data. Instead of relying on random initialization methods like Gaussian distribution, we initialize new codewords using the centroids of these features, obtained through K-means clustering. This approach expedites codebook training by providing a more informed starting point for the new codewords, allowing them to better align with the underlying data structure. As a result, this initialization strategy facilitates faster convergence and improves the model's ability to adapt to varying data distributions across silos. This strategy hugely reduces the number of training rounds required for model convergence (Details in Appendix I).

Segmented Codebooks. For complex datasets, a finite set of discrete codewords might not fully capture the diversity of image features. To bolster the robustness of our methodology, we dissect features into smaller segments to pair them with multiple codewords, thus covering the entirety of a feature vector. This segmentation exponentially increases the codeword pool, ensuring a robust representation capacity without necessitating a large-scale increase and permitting efficient K-means-based initialization. This design minimizes runtime overhead associated with larger codebooks.

3.3 Loss Function

Since we introduce learnable codewords in our method, there are two parts of the loss function. For our task, we utilize cross-entropy as the loss function. For codebook optimization, akin to the strategy employed in VQ-VAE (Van Den Oord et al., 2017), we apply a stop gradient operation for the codeword update as follows:

$$\mathcal{L}_{code} = ||sg(c) - z||_2^2 + \beta||c - sg(z)||_2^2 \tag{5}$$

where z is the image latent features, c is discrete codewords, β is a hyper-parameter to adjust the weights of two losses and $sg(\cdot)$ denotes the stop gradient function.

So, the total loss $\mathcal{L}_{UEFL}$ is the summation of $\mathcal{L}_{task}$ and $\mathcal{L}_{code}$.

3.4 Uncertainty Evaluation

As outlined in Section 3.1, evaluating model uncertainty is crucial for identifying data from heterogeneous distributions requiring supplementary codewords. In our work, we utilize Monte Carlo Dropout (MC Dropout) (Gal & Ghahramani, 2016) for uncertainty evaluation, incorporating two dropout layers into our model for regularization purposes. Unlike traditional usage where dropout layers are disabled during inference to stabilize predictions, we activate these layers during testing to generate a variety of outcomes for uncertainty analysis. This variability is quantified using predictive entropy, as described in Eq. (6), which serves to measure the prediction dispersion across different evaluations effectively.

$$e = -\sum_{class} p \log p \tag{6}$$

A low predictive entropy value signifies model confidence, whereas a high value indicates increased uncertainty. For high entropy, introducing new codewords and conducting additional training rounds are essential steps. Given the variability of uncertainty across datasets, establishing a fixed threshold is impractical. Instead, by analyzing all uncertainty values, we can benchmark against either the minimum or mean values to pinpoint target silos. Our experiments showed superior results when using the minimum value as a reference, thus guiding us to adopt the following threshold criterion:

$$e_k \leq (1+\gamma) \min_{\forall j \in 1,2,\ldots,K}(e_j), \forall k \tag{7}$$

where γ is a hyperparameter to be set.

Uncertainty decreases consistently during training, making it an effective stopping criterion for codebook extension. Besides, we also set the maximum number of iterations to 5.

4 Experimental Results

Experimental Setup. As discussed in Kairouz et al. (2021b); Zhou et al. (2023), there are two predominant forms of data heterogeneity in federated learning: feature heterogeneity and label heterogeneity. Our UEFL focuses on tacking feature heterogeneity, and we mainly discuss feature heterogeneity in this section. The discussion for label heterogeneity with dirichlet distribution and the comparison with VHL (Tang et al., 2022), FedBR (Guo et al., 2023b) are in the Appendix H.

Similar to Rotated MNIST (Ghifary et al., 2015), which creates six domains through counter-clockwise rotations of 0°, 15°, 30°, 45°, 60°, and 75° on MNIST, we employ similar technique to introduce feature heterogeneity on five different datasets: MNIST, FMNIST, CIFAR10, GTSRB, and CIFAR100, to validate our framework's robustness. In our experiments, we create three domains by counter-clockwise rotating the datasets by 0° ($\mathcal{D}_1$), -50° ($\mathcal{D}_2$), and 120° ($\mathcal{D}_3$). We sampled three data silos from each domain (*i.e.* totally 9 silos), and data silos for CIFAR100 contain 4000 images each, while the other datasets consist of 2000 images per silo. Besides the regular training with multi-domain data silos, we also test out UEFL for domain generalization (DG) task on Rotated MNIST (Ghifary et al., 2015) and PACS (Li et al., 2017) datasets, which contains four distinct domains: art painting (A), cartoon (C), photo (P), and sketch (S).

For RGB datasets like GTSRB, CIFAR10, and CIFAR100, we adopt a pretrained VGG16 model in multi-domain training. In contrast, for grayscale datasets such as MNIST and FMNIST, lacking pretrained models, we design a convolutional network comprising three ResNet blocks, training it from scratch. And for DG, we adopt a pretrained ResNet18 for both datasets. Initial codebook sizes are set to 32 for MNIST and 64 for the remaining datasets, with an equivalent number of codewords added in each subsequent iteration. While additional iterations may converge within 5 rounds, we extend this to 20 for enhanced experimental clarity. The uncertainty evaluation is conducted 20 times using a dropout rate of 0.1, with thresholds γ set at 0.3 for MNIST, 0.1 for FMNIST, GTSRB, and CIFAR100, and 0.2 for CIFAR10, to fine-tune performance. These experiments are performed on a machine with two NVIDIA A6000 GPUs.

Evaluation Metrics. We calculate the mean Top-1 accuracy (mA) as across all silos for each distribution and all data to enable a straightforward comparison. We evaluate entropy as model uncertainty as Eq. (6). We also evaluate the perplexity (PPL) to show the utility of codewords as follows,

$$PPL = exp(-\sum_{i=1}^{N} p_i \log p_i) \tag{8}$$

where N is the number of codewords, and p_i denotes the probability of the ith codeword occurring.

Similar to mA, we evaluate mean entropy (mE) and mean perplexity (mP) across data silos.

4.1 Extensible Codebook

Discretization for Heterogeneous FL. To show the effectness of discretization to tackle the data heterogeneity in FL, we design a toy experiment on MNIST. Temporarily setting aside federated learning's privacy considerations, we directly discretized the features for each client using the distinct codebooks based on its originating domain. With this discretization of VQ-FedAvg, the mean accuracy was improved from 0.834 to 0.907 with the reduction of uncertainty, demonstrating the effectiveness of feature discretization in enhancing performance within a heterogeneous federated learning context, as shown in Fig. 3a.

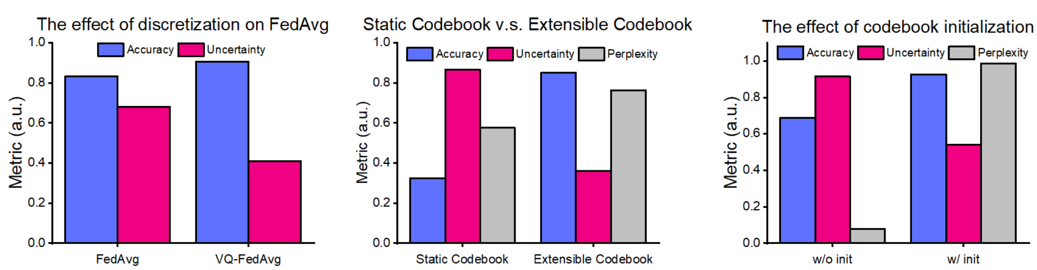

(a) Discretization works. (b) Extensible codebook is better. (c) Initialization helps.

Figure 3: **Design of extensible codebook.** (a) With the discretization (VQ-FedAvg), both accuracy and uncertainty get improved. (b) Our extensible codebook which starts from a small capacity performs better than the static large codebook. (c) With K-means initialization, the utility of codewords (*i.e.* perplexity) gets significantly improved.

Extensible Codebook v.s. Static Large Codebook. To validate our extensible codebook's superiority over starting with a large codebook, we ensured both methods ended with the same number of codewords through experiments. Results on CIFAR100 showcased in Fig. 3b demonstrate the difficulties associated with a larger initial codebook in codeword selection for image features. Conversely, gradually expanding the codebook significantly improved codeword differentiation, yielding better outcomes, such as enhanced accuracy (from 0.13 to 0.34), reduced uncertainty (0.78 vs. 1.66 for the static approach), and increased utilization of codewords.

Codebook Initialization. Section 3.1 highlights our UEFL's capability for efficient codeword initialization via K-means, utilizing features from a finetuned encoder. The efficacy of initialization is validated in Fig. 3c with results from the MNIST dataset, showing enhancements across all metrics.

4.2 UEFL FOR MULTI-DOMAIN LEARNING

Table 1: **UEFL outperforms all baselines on heterogeneous data.** DisTrans lacks a Dropout layer, rendering it incapable of evaluating uncertainty. CIFAR100* exhibits poor performance due to the highly heterogeneous experimental setup. Results for lower heterogeneity are in Appendix B.1.

Methods	**Data**	**MNIST**		**FMNIST**		**GTSRB**		**CIFAR10**		**CIFAR100***	
		mA	mE	mA	mE	mA	mE	mA	mE	mA	mE
FedAvg	$\mathcal{D}_1$	0.874	0.212	0.801	0.246	0.670	0.623	0.676	0.172	0.110	1.74
	$\mathcal{D}_2$	0.848	0.231	0.825	0.232	0.677	0.634	0.622	0.178	0.072	1.86
	$\mathcal{D}_3$	0.618	0.377	0.784	0.341	0.634	0.652	0.553	0.183	0.083	2.13
	All	0.780	0.273	0.803	0.273	0.660	0.636	0.617	0.177	0.088	1.91
DisTrans	$\mathcal{D}_1$	0.856	-	0.721	-	0.898	-	0.721	-	0.289	-
	$\mathcal{D}_2$	0.799	-	0.705	-	0.900	-	0.719	-	0.261	-
	$\mathcal{D}_3$	0.789	-	0.694	-	0.897	-	0.659	-	0.251	-
	All	0.815	-	0.707	-	0.898	-	0.699	-	0.267	-
UEFL (Ours)	$\mathcal{D}_1$	0.951	0.120	0.857	0.147	0.95	0.0196	0.776	0.0192	0.362	0.728
	$\mathcal{D}_2$	0.885	0.196	0.848	0.188	0.964	0.0206	0.713	0.0245	0.335	0.624
	$\mathcal{D}_3$	0.924	0.131	0.845	0.167	0.911	0.0314	0.671	0.0229	0.282	0.612
	All	**0.920**	**0.149**	**0.850**	**0.167**	**0.942**	**0.0239**	**0.720**	**0.0222**	**0.326**	**0.655**

We conducted comparative experiments on five datasets with introduced feature heterogeneity against leading algorithms, specifically the baseline Federated Averaging (FedAvg) (McMahan et al., 2017) and DisTrans (Yuan et al., 2022). For accuracy comparison, DisTrans generally exhibits better performance than FedAvg, making it our primary point of comparison. Regarding uncertainty comparison, because DisTrans lacks Dropout layers, precluding uncertainty evaluation, we exclusively compare uncertainty metrics with FedAvg. Deep Ensembles method is discussed in Appendix D.

Performance. The results in Table 1 provide a comprehensive comparison, illustrating that our UEFL surpasses all other state-of-the-art (SOTA) methods in both accuracy and uncertainty reduction. Specifically, UEFL improves accuracy over FedAvg by 17.94% and DisTrans by 12.88% for the $\mathcal{D}_3$ distribution of the MNIST dataset. And for uncertainty, our approach reduces uncertainty by 45.42% for the MNIST dataset's $\mathcal{D}_3$ distribution. Overall, our UEFL achieves accuracy improvements ranging from 3% to 22.1% over DisTrans. Our UEFL improves uncertainty compared to FedAvg, achieving reductions by 38.83%-96.24%. Figs. 4a and 4b details performance across individual data silos, highlighting our UEFL's effectiveness in elevating the accuracy of last three silos and degrading the uncertainty.

Codewords Perplexity. Fig. 4c presents a perplexity comparison between our UEFL and FedAvg, illustrating enhanced codebook utilization after assigning new codewords to $\mathcal{D}_3$. This adjustment not only benefits $\mathcal{D}_3$ but also improves the codebook utilization for $\mathcal{D}_1$ and $\mathcal{D}_2$.

Computation Overhead. Our approach introduces only a small codebook, thus incurring negligible memory and computational overheads. Specifically, for the CIFAR10 dataset, the parameter count for the baseline FedAvg model is 14.991M, whereas our UEFL model slightly increases to 15.491M, indicating a tiny memory increment of 3.34%. In terms of runtime, UEFL also exhibits a minimal increase from 16.154ms to 16.733ms (3.58% increase). These findings underscore UEFL's suitability for deployment on edge devices. More details are included in Appendix F.

4.3 UEFL FOR DOMAIN GENERALIZATION

For domain generalization (DG) task, the trained model needs to be evaluated on an out-of-distribution domain and we follow the evaluation method in (Nguyen et al., 2022; Guo et al., 2023a). Specifically, we perform “leave-one-domain-out” experiments, where we choose one domain as the target domain, train the model on all remaining domains, and evaluate it on the chosen domain. Each source domain is treated as a client.

As shown in Table 2, our UEFL enhanced mean accuracy on the RotatedMNIST dataset, elevating it from 0.945 to 0.953. This performance exceeds that of FedSR (Nguyen et al., 2022) at 0.947 and FedIIR (Guo et al., 2023a) at 0.95. Similarly, on the PACS dataset, UEFL improved mean accuracy from 0.803 to 0.8453, surpassing FedSR’s 0.834 and FedIIR’s 0.837. These results underscore UEFL’s efficacy in tackling feature heterogeneity and superior performance on the federated domain generalization task, beating state-of-the-art methods.

Table 2: **Comparison with different methods for DG.** Results are on six domains of Rotated MNIST, four domains of PACS and their average. Our approach is compared with baselines: FedAvg(McMahan et al., 2017), FedSR(Nguyen et al., 2022), FedIIR(Guo et al., 2023a).

Methods	Rotated MNIST							PACS				
	$\mathcal{M}_0$	$\mathcal{M}_{15}$	$\mathcal{M}_{30}$	$\mathcal{M}_{45}$	$\mathcal{M}_{60}$	$\mathcal{M}_{75}$	**Ave.**	A	C	P	S	**Ave.**
FedAvg	82.7	98.2	99	99.1	98.2	89.9	94.5	78	73	92	79	80.3
FedSR	84.2	98.0	98.9	99.0	98.3	90.0	94.7	83	75	94	82	83.4
FedIIR	83.8	98.2	99.1	99.1	98.5	90.8	95.0	83	76	94	82	83.7
UEFL (ours)	88.1	97.3	97.6	97.8	97.9	93.2	**95.3**	81	80	94	82	**84.5**

4.4 ABLATION STUDY

Imbalanced Clients. We constructed an experimental setup with three data silos from $\mathcal{D}_1$ and one each from $\mathcal{D}_2$ and $\mathcal{D}_3$, totaling five silos. Our UEFL can also improve both accuracy (from 0.508 to 0.828) and uncertainty (from 0.256 to 0.105) in this scenario. Detailed results are in Appendix J.

Large Number of Clients. We follow the settings in Guo et al. (2023a) to further segment the five training domains of Rotated MNIST into 50 sub-domains, each representing an individual client. Our UEFL achieves the best mean accuracy of 0.9342, surpassing the performances of FedAvg at 0.908, FedSR at 0.912, and FedIIR at 0.93 as shown in Table 4, suggesting our UEFL is scalable for a larger number of clients.

Number of codewords and segments. We investigate the impact of varying the number of initialized codewords in our extensible codebook, to balance accuracy with runtime efficiency in K-means initialization. In Fig. 5a for GTSRB, initializing with 32 codewords provides comparable accuracy and uncertainty metrics. For more complex datasets, we enhance selection capacity using code-

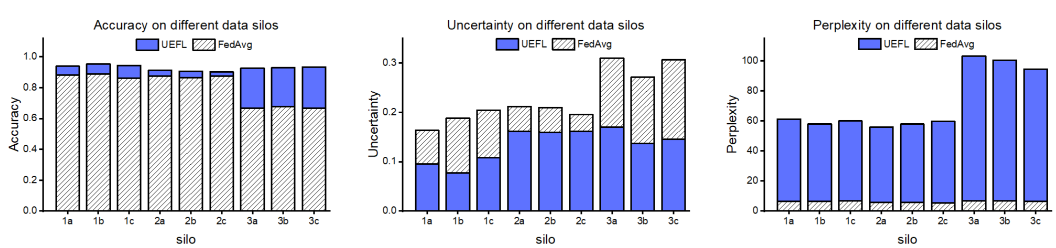

(a) Accuracy comparison. (b) Uncertainty comparison. (c) Perplexity comparison.

Figure 4: **Detailed comparison for all data silos.** Experiments are on MNIST. $\mathcal{D}_3$ presents much lower accuracy and higher uncertainty compared to $\mathcal{D}_1$, $\mathcal{D}_2$ for FedAvg. And the perplexity results show that our UEFL assigns new codewords to $\mathcal{D}_3$ to improve the performance.

Table 3: UEFL is scalable for 50 clients and beats all SOTA methods by comparing with baselines: FedAvg(McMahan et al., 2017), FedSR(Nguyen et al., 2022), FedIIR(Guo et al., 2023a).

Methods	**#Clients**	**Backbone**	**Domains**						**Average**
			$\mathcal{M}_0$	$\mathcal{M}_{15}$	$\mathcal{M}_{30}$	$\mathcal{M}_{45}$	$\mathcal{M}_{60}$	$\mathcal{M}_{75}$	
FedAvg	50	ResNet18	77.9	95.9	96.9	97	96	81.2	90.8
FedSR	50	ResNet18	78.3	95.7	96.3	97.1	96	84	91.2
FedIIR	50	ResNet18	84	96.8	97.7	97.7	97.4	84.5	93
UEFL (ours)	50	ResNet18	86.4	95.5	96.4	96.9	94.7	90.6	**93.42**

Table 4: Results show our UEFL is also scalable for 100 clients and beats all SOTA methods following the experimental setup in FedCR (Zhang et al., 2023).

Methods	**#Clients**	**EMNIST-L**	**FMNIST**	**CIFAR10**	**CIFAR100**
FedAvg (McMahan et al., 2017)	100	95.89	88.15	76.83	32.08
FedSR (Nguyen et al., 2022)	100	86.22	85.55	61.47	40.82
FedCR (Zhang et al., 2023)	100	97.47	93.78	84.74	62.96
UEFL (ours)	100	**98.29**	**93.93**	**86.11**	**63.37**

word segmentation. Fig. 5b demonstrates that segmenting codewords into 4 parts leads to enhanced performance on CIFAR100.

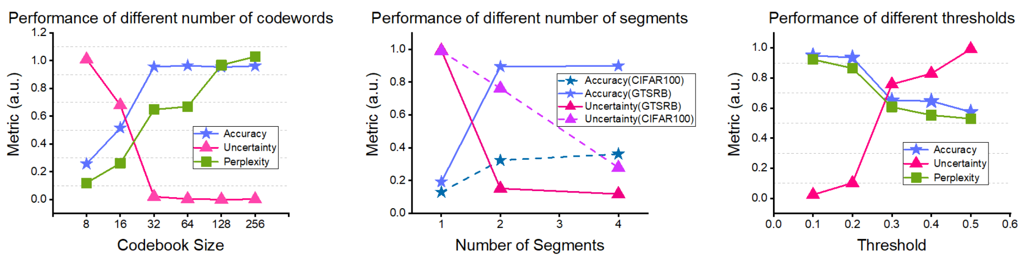

(a) 32 codewords are sufficient. (b) Codeword segments. (c) Uncertainty threshold.

Figure 5: (a) 32 initialized codewords are sufficient for our UEFL. (b) We need 2 segments for GTSRB but 4 segments for CIFAR100. (c) Overall, a smaller threshold performs better.

Uncertainty Threshold. In our UEFL, the uncertainty evaluator plays a pivotal role in identifying heterogeneous data without needing direct data access, with the threshold selection being critical. As illustrated in Fig. 5c, a lower threshold imposes stricter criteria, pushing the model to achieve higher performance. However, it's important to recognize that beyond a certain point, further reducing the threshold may not significantly enhance outcomes but will increase computational overhead. Thus, in such cases, there is a trade-off between runtime and performance.

5 Conclusion

In this work, we address the challenge of data heterogeneity among silos within federated learning setting by introducing an innovative solution: an extensible codebook designed to map distinct data distributions using varied codeword pools. Our proposed framework, Uncertainty-Based Extensible-Codebook Federated Learning (UEFL), leverages this extensible codebook through an iterative process that adeptly identifies data from unknown distributions via uncertainty evaluation and enriches the codebook with newly initialized codewords tailored to these distributions. The iterative nature of UEFL, coupled with efficient codeword initialization using K-means, ensures codewords are closely matched with the actual data distribution, thereby expediting model convergence. This approach allows UEFL to rapidly adjust to new and unseen data distributions, enhancing adaptability. Our comprehensive evaluation across various prominent datasets showcases UEFL's effectiveness.

REFERENCES

Naman Agarwal, Peter Kairouz, and Ziyu Liu. The skellam mechanism for differentially private federated learning. *Advances in Neural Information Processing Systems*, 34:5052–5064, 2021.

Hongjoon Ahn, Sungmin Cha, Donggyu Lee, and Taesup Moon. Uncertainty-based continual learning with adaptive regularization. *Advances in neural information processing systems*, 32, 2019.

Charles Blundell, Julien Cornebise, Koray Kavukcuoglu, and Daan Wierstra. Weight uncertainty in neural network. In *International conference on machine learning*, pp. 1613–1622. PMLR, 2015.

Fei Chen, Mi Luo, Zhenhua Dong, Zhenguo Li, and Xiuqiang He. Federated meta-learning with fast convergence and efficient communication. *arXiv preprint arXiv:1802.07876*, 2018.

Qi Chen, Amanda Whitbrook, Uwe Aickelin, and Chris Roadknight. Data classification using the dempster–shafer method. *Journal of Experimental & Theoretical Artificial Intelligence*, 26(4): 493–517, 2014.

Michael W Dusenberry, Dustin Tran, Edward Choi, Jonas Kemp, Jeremy Nixon, Ghassen Jerfel, Katherine Heller, and Andrew M Dai. Analyzing the role of model uncertainty for electronic health records. In *Proceedings of the ACM Conference on Health, Inference, and Learning*, pp. 204–213, 2020.

Yarin Gal and Zoubin Ghahramani. Dropout as a bayesian approximation: Representing model uncertainty in deep learning. In *international conference on machine learning*, pp. 1050–1059. PMLR, 2016.

Jakob Gawlikowski, Cedrique Rovile Njieutcheu Tassi, Mohsin Ali, Jongseok Lee, Matthias Humt, Jianxiang Feng, Anna Kruspe, Rudolph Triebel, Peter Jung, Ribana Roscher, et al. A survey of uncertainty in deep neural networks. *arXiv preprint arXiv:2107.03342*, 2021.

Robin C Geyer, Tassilo Klein, and Moin Nabi. Differentially private federated learning: A client level perspective. *arXiv preprint arXiv:1712.07557*, 2017.

Muhammad Ghifary, W Bastiaan Kleijn, Mengjie Zhang, and David Balduzzi. Domain generalization for object recognition with multi-task autoencoders. In *Proceedings of the IEEE international conference on computer vision*, pp. 2551–2559, 2015.

Avishek Ghosh, Jichan Chung, Dong Yin, and Kannan Ramchandran. An efficient framework for clustered federated learning. *Advances in Neural Information Processing Systems*, 33:19586–19597, 2020.

Yaming Guo, Kai Guo, Xiaofeng Cao, Tieru Wu, and Yi Chang. Out-of-distribution generalization of federated learning via implicit invariant relationships. In *International Conference on Machine Learning*, pp. 11905–11933. PMLR, 2023a.

Yongxin Guo, Xiaoying Tang, and Tao Lin. Fedbr: Improving federated learning on heterogeneous data via local learning bias reduction. In *International Conference on Machine Learning*, pp. 12034–12054. PMLR, 2023b.

Andrew Hard, Kanishka Rao, Rajiv Mathews, Swaroop Ramaswamy, Françoise Beaufays, Sean Augenstein, Hubert Eichner, Chloé Kiddon, and Daniel Ramage. Federated learning for mobile keyboard prediction. *arXiv preprint arXiv:1811.03604*, 2018.

Wenke Huang, Mang Ye, and Bo Du. Learn from others and be yourself in heterogeneous federated learning. In *Proceedings of the IEEE/CVF Conference on Computer Vision and Pattern Recognition*, pp. 10143–10153, 2022.

Peter Kairouz, Ziyu Liu, and Thomas Steinke. The distributed discrete gaussian mechanism for federated learning with secure aggregation. In *International Conference on Machine Learning*, pp. 5201–5212. PMLR, 2021a.

Peter Kairouz, H Brendan McMahan, Brendan Avent, Aurélien Bellet, Mehdi Bennis, Arjun Nitin Bhagoji, Kallista Bonawitz, Zachary Charles, Graham Cormode, Rachel Cummings, et al. Advances and open problems in federated learning. *Foundations and trends® in machine learning*, 14(1–2):1–210, 2021b.

Shivam Kalra, Junfeng Wen, Jesse C Cresswell, Maksims Volkovs, and HR Tizhoosh. Decentralized federated learning through proxy model sharing. *Nature communications*, 14(1):2899, 2023.

Alex Kendall and Yarin Gal. What uncertainties do we need in bayesian deep learning for computer vision? *Advances in neural information processing systems*, 30, 2017.

Jakub Konečnỳ, H Brendan McMahan, Daniel Ramage, and Peter Richtárik. Federated optimization: Distributed machine learning for on-device intelligence. *arXiv preprint arXiv:1610.02527*, 2016.

Salem Lahlou, Moksh Jain, Hadi Nekoei, Victor Ion Butoi, Paul Bertin, Jarrid Rector-Brooks, Maksym Korablyov, and Yoshua Bengio. Deup: Direct epistemic uncertainty prediction. *arXiv preprint arXiv:2102.08501*, 2021.

Balaji Lakshminarayanan, Alexander Pritzel, and Charles Blundell. Simple and scalable predictive uncertainty estimation using deep ensembles. *Advances in neural information processing systems*, 30, 2017.

Da Li, Yongxin Yang, Yi-Zhe Song, and Timothy M Hospedales. Deeper, broader and artier domain generalization. In *Proceedings of the IEEE international conference on computer vision*, pp. 5542–5550, 2017.

Liping Li, Wei Xu, Tianyi Chen, Georgios B Giannakis, and Qing Ling. Rsa: Byzantine-robust stochastic aggregation methods for distributed learning from heterogeneous datasets. In *Proceedings of the AAAI Conference on Artificial Intelligence*, volume 33, pp. 1544–1551, 2019.

Tian Li, Anit Kumar Sahu, Maziar Sanjabi, Manzil Zaheer, Ameet Talwalkar, and Virginia Smith. On the convergence of federated optimization in heterogeneous networks. *arXiv preprint arXiv:1812.06127*, 2018.

Dianbo Liu, Alex Lamb, Kenji Kawaguchi, Anirudh Goyal, Chen Sun, Michael Mozer, and Yoshua Bengio. Discrete-valued neural communication in structured architectures enhances generalization. 2021.

Christos Louizos and Max Welling. Multiplicative normalizing flows for variational bayesian neural networks. In *International Conference on Machine Learning*, pp. 2218–2227. PMLR, 2017.

Brendan McMahan, Eider Moore, Daniel Ramage, Seth Hampson, and Blaise Aguera y Arcas. Communication-efficient learning of deep networks from decentralized data. In *Artificial intelligence and statistics*, pp. 1273–1282. PMLR, 2017.

Zachary Nado, Neil Band, Mark Collier, Josip Djolonga, Michael W Dusenberry, Sebastian Farquhar, Qixuan Feng, Angelos Filos, Marton Havasi, Rodolphe Jenatton, et al. Uncertainty baselines: Benchmarks for uncertainty & robustness in deep learning. *arXiv preprint arXiv:2106.04015*, 2021.

A Tuan Nguyen, Philip Torr, and Ser Nam Lim. Fedsr: A simple and effective domain generalization method for federated learning. *Advances in Neural Information Processing Systems*, 35:38831–38843, 2022.

Vardan Papyan, XY Han, and David L Donoho. Prevalence of neural collapse during the terminal phase of deep learning training. *Proceedings of the National Academy of Sciences*, 117(40): 24652–24663, 2020.

Zhenheng Tang, Yonggang Zhang, Shaohuai Shi, Xin He, Bo Han, and Xiaowen Chu. Virtual homogeneity learning: Defending against data heterogeneity in federated learning. In *International Conference on Machine Learning*, pp. 21111–21132. PMLR, 2022.

Aaron Van Den Oord, Oriol Vinyals, et al. Neural discrete representation learning. *Advances in neural information processing systems*, 30, 2017.

Qiang Yang, Yang Liu, Tianjian Chen, and Yongxin Tong. Federated machine learning: Concept and applications. *ACM Transactions on Intelligent Systems and Technology (TIST)*, 10(2):1–19, 2019.

Haolin Yuan, Bo Hui, Yuchen Yang, Philippe Burlina, Neil Zhenqiang Gong, and Yinzhi Cao. Addressing heterogeneity in federated learning via distributional transformation. In *European Conference on Computer Vision*, pp. 179–195. Springer, 2022.

Hao Zhang, Chenglin Li, Wenrui Dai, Junni Zou, and Hongkai Xiong. Fedcr: Personalized federated learning based on across-client common representation with conditional mutual information regularization. In *International Conference on Machine Learning*, pp. 41314–41330. PMLR, 2023.

Tianyi Zhang, Shirui Zhang, Ziwei Chen, Yoshua Bengio, and Dianbo Liu. Pmfl: Partial meta-federated learning for heterogeneous tasks and its applications on real-world medical records. In *2022 IEEE International Conference on Big Data (Big Data)*, pp. 4453–4462. IEEE, 2022.

Yue Zhao, Meng Li, Liangzhen Lai, Naveen Suda, Damon Civin, and Vikas Chandra. Federated learning with non-iid data. *arXiv preprint arXiv:1806.00582*, 2018.

Tailin Zhou, Jun Zhang, and Danny HK Tsang. Fedfa: Federated learning with feature anchors to align features and classifiers for heterogeneous data. *IEEE Transactions on Mobile Computing*, 2023.

A DISCRETIZATION FOR GENERALIZATION

Theoretically, the inclusion of the discretization process offers two key advantages: (1) enhanced noise robustness, and (2) reduced underlying dimensionality. These benefits are demonstrated in the following two theorems. (Liu et al., 2021).

Notation: $\boldsymbol{h}$ is input vector, $\boldsymbol{h} \in \mathcal{H} \in \mathcal{R}^m$. L is the size of codebook, G is the number of segments, $q(\cdot)$ is discretization process, $\phi(\cdot)$ is any function (model). Given any family of sets $S = \{S_1, ..., S_K\}$ with $S_1, ..., S_K \subseteq \mathcal{H}$, we define ϕ_k^S by $\phi_k^S = \mathbb{1}\{\boldsymbol{h} \in S_k\}\phi(\boldsymbol{h})$ for all $k \in [K]$, where $[K] = \{1, ..., K\}$. And we denote by $(Q_k)_{k \in [L^G]}$ all the codewords.

Theorem 1: (with discretization) *Let* $S_k = \{Q_k\}$ *for all* $k \in [L^G]$. *Then, for any* $\delta > 0$, *with probability at least* $1 - \delta$ *over an iid draw of* n *examples* $(\boldsymbol{h}_i)_{i=1}^n$, *the following holds for any* $\phi : \mathcal{R}^m \to \mathcal{R}$ *and all* $k \in [L^G]$: *if* $|\phi_k^S(\boldsymbol{h})| \leq \alpha$ *for all* $\boldsymbol{h} \in \mathcal{H}$, *then*

$$\left| \mathbb{E}_{\boldsymbol{h}}[\phi_k^S(q(\boldsymbol{h}, L, G))] - \frac{1}{n}\sum_{i=1}^{n} \phi_k^S(q(\boldsymbol{h}_i, L, G)) \right| = \mathcal{O}(\alpha\sqrt{\frac{G\ln(L) + \ln(2/\delta)}{2n}}), \tag{9}$$

where no constant is hidden in $\mathcal{O}$.

Theorem 2: (without discretization) *Assume that* $||\boldsymbol{h}||_2 \leq R_{\mathcal{H}}$ *for all* $\boldsymbol{h} \in \mathcal{H} \in \mathcal{R}^m$. *Fix* $\mathcal{C} \in \mathrm{argmin}_{\overline{\mathcal{C}}}\{|\overline{\mathcal{C}}| : \overline{C} \subseteq \mathcal{R}^m, \mathcal{H} \subseteq \cup_{c \in \overline{\mathcal{C}}} \mathcal{B}[c]\}$ *where* $\mathcal{B}[\boldsymbol{c}] = \{\boldsymbol{x} \in \mathcal{R}^m : ||\boldsymbol{x} - \mathbf{c}||_2 \leq R_{\mathcal{H}}/(2\sqrt{n})\}$. *Let* $S_k = \mathcal{B}[\boldsymbol{c}_k]$ *for all* $k \in [|\mathcal{C}|]$ *where* $\boldsymbol{c}_k \in \mathcal{C}$ *and* $\cup_k\{\boldsymbol{c}_k\} = \mathcal{C}$. *Then, for any* $\delta > 0$, *with probability at least* $1 - \delta$ *over an iid draw of* n *examples* $(\boldsymbol{h}_i)_{i=1}^n$,*the following holds for any* $\phi : \mathcal{R}^m \to \mathcal{R}$ *and all* $k \in [|\mathcal{C}|]$: *if* $|\phi_k^S(\boldsymbol{h})| \leq \alpha$ *for all* $\boldsymbol{h} \in \mathcal{H}$ *and* $|\phi_k^S(\boldsymbol{h}) - \phi_k^S(\boldsymbol{h}')| \leq \varsigma_k ||\boldsymbol{h} - \boldsymbol{h}'||_2$ *for all* $\boldsymbol{h}, \boldsymbol{h}' \in S_k$, *for all* $\boldsymbol{h}, \boldsymbol{h}' \in S_k$, *then*

$$\left| \mathbb{E}_{\boldsymbol{h}}[\phi_k^S(\boldsymbol{h})] - \frac{1}{n}\sum_{i=1}^{n} \phi_k^S(\boldsymbol{h}_i) \right| = \mathcal{O}(\alpha\sqrt{\frac{m\ln(4\sqrt{nm}) + \ln(2/\delta)}{2n}} + \frac{\overline{\varsigma_k} R_{\mathcal{H}}}{\sqrt{n}}), \tag{10}$$

where no constant is hidden in $\mathcal{O}$ *and* $\overline{\varsigma_k} = \varsigma_k(\frac{1}{n}\sum_{i=1}^n \mathbb{1}\{h_i \in \mathcal{B}[c_k]\})$.

Based on these two theorems, we can determine that the performance gap between training and test data is smaller when discretization is applied, due to the following two points:

- There is an additional error without discretization (i.e. $\frac{\overline{\varsigma_k} R_{\mathcal{H}}}{\sqrt{n}}$) in the bound of Theorem 2. This error disappears with discretization in the bound of Theorem 1 as the discretization process reduces the sensitivity to noise.
- The discretization process reduces the underlying dimensionality of $m\ln(4\sqrt{nm})$ without discretization (in Theorem 2) to that of $G\ln(L)$ with discretization (in Theorem 1). Since the number of discretization heads G (eg. G is 1, 2, or 4 in our case) is always much smaller than the number of dimensions m, the inequality $G\ln(L) \leq m\ln(4\sqrt{nm})$ consistently holds.

B Different data heterogeneity for UEFL

B.1 Lower Data heterogeneity on CIFAR100

To provide a detailed comparison with the baseline, we used a VGG16 backbone to test CIFAR100 under multiple settings: (1) Local Training: all data trained together without a distributed setting; (2) FedAvg (w/o hete): CIFAR100 split into 5 clients, each with 10,000 images, to evaluate FedAvg performance; (3) FedAvg (w/ hete): images for the 5 clients were rotated by -30°, -15°, 0°, 15°, and 30°, respectively, to introduce data heterogeneity, and FedAvg performance was evaluated; (4) UEFL (w/ hete): tested under the same heterogeneous setup. We trained models from scratch and with pre-trained weights. Results are presented in Table 5, showing that UEFL consistently outperforms FedAvg in both cases.

Table 5: Under lower data heterogeneity on CIFAR100, UEFL continues to outperform FedAvg for both training from scratch and using pre-trained weights.

Training Strategy	Local training	FedAvg (w/o hete)	FedAvg (w/ hete)	UEFL (w/ hete)
From scratch	0.3852	0.2447	0.0852	0.1062
Pre-trained	0.6604	0.6496	0.5005	0.5619

B.2 Different data heterogeneity on CIFAR100

By progressively increasing the rotation angles to simulate greater data heterogeneity, we evaluated UEFL's performance under varying levels of heterogeneity. As shown in Table 6, while overall performance decreases with higher heterogeneity, UEFL consistently outperforms FedAvg, with the performance gap widening as heterogeneity increases, demonstrating UEFL's superiority in addressing data heterogeneity.

Table 6: With different rotation angles, UEFL keep outperforms FedAvg.

Rotation Angles	FedAvg	UEFL
{-10°, -5°, 0°, 5°, 10°}	0.5935	0.6232
{-20°, -10°, 0°, 10°, 20°}	0.5469	0.6039
{-30°, -15°, 0°, 15°, 30°}	0.5106	0.56
{-40°, -20°, 0°, 20°, 40°}	0.4799	0.5311
{-50°, -25°, 0°, 25°, 50°}	0.4494	0.5074
{-60°, -30°, 0°, 30°, 60°}	0.4368	0.4939
{-70°, -35°, 0°, 35°, 70°}	0.4188	0.4737

C Optimal training epochs of baselines

To fully demonstrate the efficacy of our UEFL, besides evaluating baselines with the same total training epochs as UEFL, we remove the additional training epochs from UEFL iterations and obtain the optimal performance, for more fair comparison.

Table 7: UEFL outperforms all baselines without additional training epochs.

Methods	**MNIST**		**FMNIST**		**GTSRB**		**CIFAR10**		**CIFAR100**	
	mA	mE	mA	mE	mA	mE	mA	mE	mA	mE
FedAvg	0.782	0.261	0.801	0.289	0.657	0.645	0.618	0.173	0.093	1.74
UEFL (Ours)	**0.920**	**0.149**	**0.850**	**0.167**	**0.942**	**0.0239**	**0.720**	**0.0222**	**0.326**	**0.655**

D Deep Ensembles

We evaluated Deep Ensembles by creating 5 ensembles to assess uncertainty for our method. Table 8 shows a comparison between Deep Ensembles and Monte Carlo Dropout. From the results, we observe that the accuracy when using Deep Ensembles is quite similar to Monte Carlo Dropout, apart from the stochastic variations. This is expected, as the accuracy is not directly impacted by the choice of uncertainty evaluation method. However, the uncertainty values for Deep Ensembles are higher than those for Monte Carlo Dropout, likely due to the use of only 5 ensembles for evaluation to reduce computational time. In conclusion, while the accuracy is comparable, Deep Ensembles require significantly more computational resources due to the need to train multiple networks. Therefore, Monte Carlo Dropout is a more efficient and suitable choice for our approach.

Table 8: Comparison of Deep Ensembles and Monte Carlo Dropout for uncertainty evaluation.

Methods	**MNIST**		**FMNIST**		**GTSRB**		**CIFAR10**		**CIFAR100**	
	mA	mE	mA	mE	mA	mE	mA	mE	mA	mE
Monte Carlo Dropout	0.920	0.149	0.850	0.167	0.942	0.0239	0.720	0.0222	0.326	0.655
Deep Ensemble	0.926	0.211	0.853	0.289	0.940	0.041	0.717	0.043	0.331	0.873

E Neural Collapse

We conducted experiments on MNIST and CIFAR-100 based on the framework presented in (Papyan et al., 2020). According to the paper, when training continues until the training error reaches 0 (*i.e.* training accuracy exceeds 99.9% for MNIST/CIFAR-10), the Terminal Phase of Training (TPT) begins, during which neural collapse (NC) emerges. To validate this, we first conducted local training by training on all data together. Our results confirmed the paper's claim that additional training beyond the zero-error point leads to improved performance. We then extended these experiments to the federated learning setting. The detailed results are presented in Table 9.

From these experiments, we observed the following findings: 1. The dropout layer must be removed; otherwise, the training accuracy cannot exceed 99.9% (e.g., the final training accuracy for MNIST is limited to 96% with dropout). 2. Compared to local training, more training epochs are required to reach the TPT in federated learning. For example, on CIFAR-100 with data heterogeneity, federated learning requires 44 rounds of training (44 × 5 epochs), while local training achieves TPT in 38 epochs. 3. Although neural collapse yields improved performance, UEFL consistently outperforms it, especially on more complex datasets like CIFAR-100. This is partly because removing dropout layers for neural collapse increases the risk of overfitting.

Table 9: Comparison with neural collapse (NC).

Method	MNIST	CIFAR100
zero-error	0.9375	0.3473
last epoch (NC)	0.9584	0.3482
UEFL (Ours)	0.9778	0.5074

F COMPUTATION COST

Table 10 compares FedAvg and UEFL. The parameter count for UEFL in this table represents the final model size, including 256 codewords after two iterations starting from 64. In our experiments, 256 is the largest final codebook size across all datasets. For simpler datasets like MNIST, UEFL demonstrates an even lower computation cost.

Table 10: With different rotation angles, UEFL keep outperforms FedAvg.

Method	#Params (M)	CPU runtime (ms)	GPU runtime (ms)
FedAvg	14.991	16.102	16.154
UEFL (Ours)	15.491	16.611	16.733

G CONVERGENCE CURVES

For the experiments on the CIFAR10 dataset, in Fig. 6, at round 40, after we assign new codewords, rapid performance gains are evident. Remarkably, the training process demonstrates swift convergence, typically within just five rounds. For illustrative clarity and to underscore the differential impact, we extend the training to 20 rounds in subsequent iterations, showcasing the accelerated and effective adaptation of our approach. In addition, after 60 rounds, even if we keep adding new codewords, the increased perplexity denotes a higher utilization of the codebook. However, there is no significant improvement in accuracy or uncertainty. Fig. 6 also shows a large boost with our UEFL on MNIST.

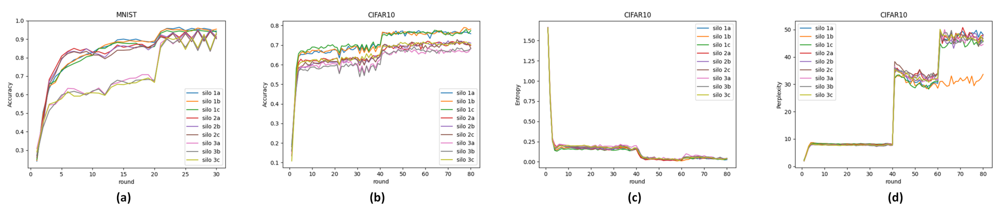

Figure 6: **Learning curves of MNIST and CIFAR10.** (a) Accuracy of MNIST. (b) Accuracy of CIFAR10. (c) Uncertainty of CIFAR10. (d) Perplexity of CIFAR10.

For the experiments on the FMNIST and GTSRB datasets, as depicted in Fig. 7, we introduce new codewords to the codebook only once. Notably, there is a clear "performance jump" evident in all six figures, showcasing the rapid adaptation of our UEFL to new data distributions.

H OUR UEFL FOR LABEL HETEROGENEITY

Similar to (Tang et al., 2022; Guo et al., 2023b), we introduce label heterogeneity with dirichlet distribution ($\alpha = 0.1$). The results in Table 11 show that our UEFL can also tackle the label heterogeneity when compared to FedAvg and performs better than VHL for CIFAR10 even if it cannot perform as well as FedBR.

Table 11: **Comparison with different methods on data with label heterogeneity.**

Method	**FMNIST**			**CIFAR10**			
	FedAvg	VHL	UEFL (ours)	FedAvg	VHL	FedBR	UEFL (ours)
mA	87.45	91.52	90.59	58.99	61.23	64.61	62.67

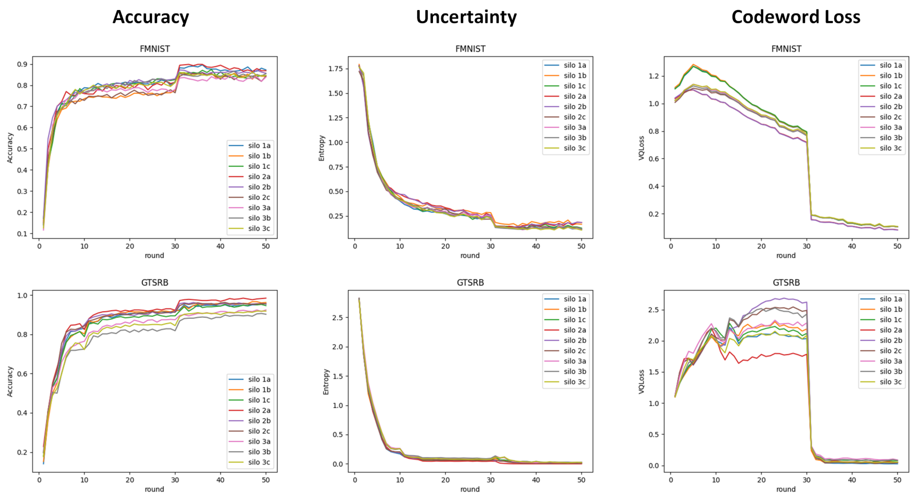

Figure 7: **Learning curves of FMNIST and GTSRB.** (left) Accuracy results. (mid) Uncertainty results. (right) codeword loss results.

I K-MEANS INITIALIZATION

Fig. 8 illustrates this concept: gray points represent features from the trained encoder, clustered according to their data distributions. While direct data access is restricted, differentiation by uncertainty allows us to identify and utilize the centroids of these clusters via K-means for codeword initialization.

And to bolster the robustness of our methodology, we dissect features into smaller segments—using factors like 2 or 4—to pair them with multiple codewords, thus covering the entirety of a feature vector as illustrated in Figure 3. This segmentation exponentially increases the codeword pool to n^2 or n^4, ensuring a robust representation capacity.

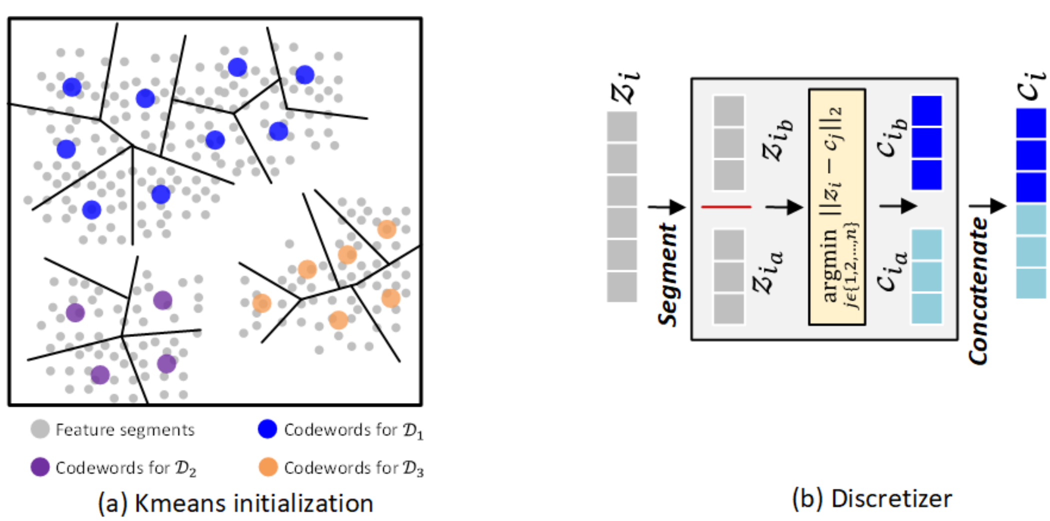

Figure 8: (a) Kmeans initialization for heterogeneous data silos. (b) Workflow of discretizer.

Table 12: Our UEFL improves the performance of unbalanced data.

Data	Silo	FedAvg		UEFL	
		Acc	Entropy	Acc	Entropy
$\mathcal{D}_1$	s_{1_a}	0.964	0.0312	0.952	0.0291
	s_{1_b}	0.936	0.0252	0.974	0.0170
	s_{1_c}	0.964	0.0499	0.944	0.0308
$\mathcal{D}_2$	s_{2_a}	0.796	0.1477	**0.836**	**0.1261**
$\mathcal{D}_3$	s_{3_a}	0.508	0.2560	**0.828**	**0.1048**

J Imbalanced Clients

As shown in Table 12, our UEFL also works for imbalanced data silos when there are three clients sampled from the same domain. Both accuracy and uncertainty get improved, especially for the third domain.

K UEFL Optimization

Number of Codewords. We investigate the impact of varying the number of initialized codewords within our extensible codebook in Table 13, aiming to strike a balance between achieving competitive accuracy and optimizing the runtime efficiency of the K-means initialization. Our findings, for the GTSRB dataset, reveal that starting with 32 or 64 codewords offers comparable accuracy and uncertainty metrics to larger codebooks, while significantly enhancing the efficiency of the K-means initialization. This efficiency highlights the efficacy of our proposed approach.

In addition, for more complex datasets, requiring a broader representation of image features but with minimal initialization time, we employ codeword segmentation to enhance selection capacity efficiently. We explore the impact of segmentation factors of 1, 2, and 4, starting with 16 codewords for GTSRB and 32 for CIFAR100. Our findings indicate that, particularly for CIFAR100, splitting vectors into 4 segments with only 32 initialized codewords achieves impressive performance. Similarly, for GTSRB, segmentation into 2 parts is adequate for effective image feature representation.

#Codes	Data	$\mathcal{L}_{\text{code}}\downarrow$	mP↑	mE↓	mA↑	codebook growth
8	$\mathcal{D}_1$	3.61	4.78	2.02	0.257	$8 \rightarrow 16 \rightarrow 32 \rightarrow 64$
	$\mathcal{D}_2$	3.68	4.86	2.01	0.265	
	$\mathcal{D}_3$	3.38	4.81	2.03	0.249	
16	$\mathcal{D}_1$	3.41	10.46	1.36	0.515	$16 \rightarrow 32 \rightarrow 64$
	$\mathcal{D}_2$	3.55	10.54	1.37	0.506	
	$\mathcal{D}_3$	3.23	10.61	1.39	0.486	
32	$\mathcal{D}_1$	0.127	25.91	0.0412	0.956	$32 \rightarrow 64 \rightarrow 128$
	$\mathcal{D}_2$	0.0885	25.42	0.0313	0.966	
	$\mathcal{D}_3$	0.178	26.37	0.117	0.911	
64	$\mathcal{D}_1$	0.0975	26.79	0.0086	**0.965**	$64 \rightarrow 128$
	$\mathcal{D}_2$	0.0853	26.32	0.0084	**0.974**	
	$\mathcal{D}_3$	0.1907	27.23	0.0166	**0.926**	
128	$\mathcal{D}_1$	0.0512	38.73	-	0.954	$128 \rightarrow 256$
	$\mathcal{D}_2$	0.0453	34.16	-	0.968	
	$\mathcal{D}_3$	0.0726	43.42	-	0.917	
256	$\mathcal{D}_1$	0.0543	41.20	0.0043	0.962	$256 \rightarrow 512$
	$\mathcal{D}_2$	0.0301	38.96	0.0054	0.959	
	$\mathcal{D}_3$	0.0577	50.57	0.0103	0.904	

Table 13: **Number of codewords.** Experiment are on GTSRB dataset. ”-” denotes value close to 0.

Table 14: The experiments were conducted on the MNIST dataset with 128 initialized codewords and segmentation factor 1. The model with K-means initialization outperforms without it.

Codebook	**Data**	$\mathcal{L}_{\mathbf{code}}$	**mP**	**mE**	**mA**
w/o init	$\mathcal{D}_1$	0.6202	6.26	0.125	0.888
	$\mathcal{D}_2$	0.6063	5.99	0.296	0.554
	$\mathcal{D}_3$	0.6096	5.35	0.267	0.622
w/ init	$\mathcal{D}_1$	0.0862	59.64	0.0935	0.945
	$\mathcal{D}_2$	0.0785	57.58	0.1604	0.906
	$\mathcal{D}_3$	0.0779	99.38	0.1509	0.929

Codebook Initialization. Section 3.1 highlights our UEFL framework's capability for efficient codeword initialization via K-means, utilizing features from a trained encoder. The efficacy of K-means initialization is validated in Table 14 with results from the MNIST dataset, showing enhancements across all metrics.

Extensible Codebook v.s. Static Large Codebook. To validate our extensible codebook's superiority over starting with a large codebook, we ensured both methods ended with the same number of codewords through experiments. For the CIFAR100 dataset, the extensible codebook was initially set to 128 codewords and expanded twice, while the static codebook was fixed at 512 codewords. Results showcased in Table 15 demonstrate the difficulties associated with a larger initial codebook in codeword selection for image features. Conversely, gradually expanding the codebook significantly improved codeword differentiation, yielding better outcomes, such as enhanced accuracy (0.375 for Domain 1) and reduced uncertainty (0.78 vs. 1.66 for the static approach). In addition, perplexity results reveal increased utilization of our extensible codebook, offering clear evidence of our design's superiority.

Table 15: Our extensible codebook (Extend) outperforms the static larger codebook (Static) on all evaluation metrics.

Codebook	**Data**	$\mathcal{L}_{\mathbf{code}}$	**mP**	**mE**	**mA**
Static	$\mathcal{D}_1$	3.10	17.54	1.66	0.142
	$\mathcal{D}_2$	2.91	17.41	1.76	0.135
	$\mathcal{D}_3$	2.63	16.82	1.76	0.112
Extend	$\mathcal{D}_1$	1.28	19.31	0.7822	0.375
	$\mathcal{D}_2$	0.976	27.42	0.6665	0.341
	$\mathcal{D}_3$	0.978	22.00	0.7112	0.304

Different Uncertainty Threshold. In our UEFL, the uncertainty evaluator plays a pivotal role in identifying heterogeneous data without needing direct data access, with the threshold selection being critical. An optimal threshold enhances the model's ability to distinguish between data silos, leading to quicker convergence. As illustrated in Fig. 9, a lower threshold imposes stricter criteria, pushing the model to achieve higher precision, thereby improving performance metrics. However, it's important to recognize that beyond a certain point, further reducing the threshold may not significantly enhance outcomes but will increase computational overhead. Thus, in such cases, there is a trade-off between runtime and performance.

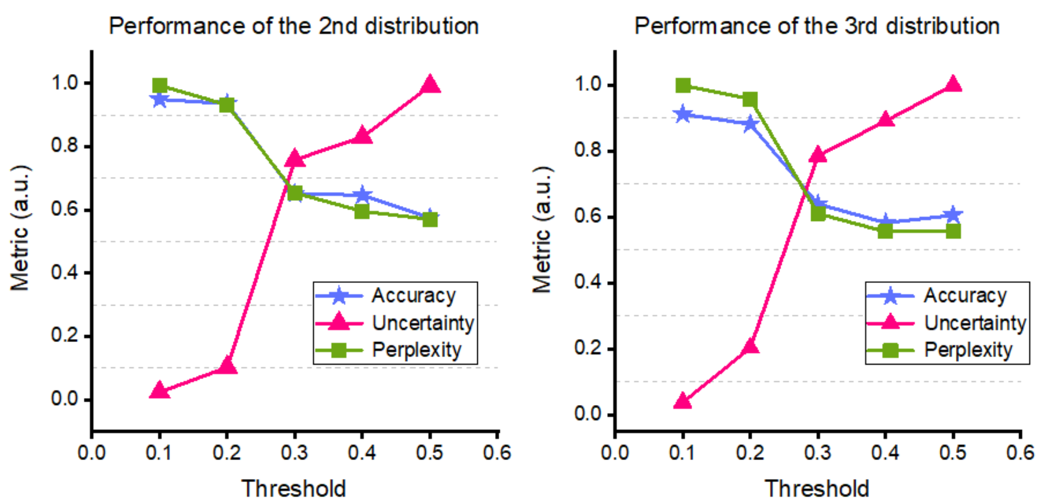

Figure 9: Results on GTSRB dataset with 64 initialized codewords with segment 1. Overall, a smaller threshold performs better.